Amplitude and Phase Imbalance Calibration for Space-Based Precision Direction Finding Systems

José A. de Souza Melo, 1, Lucas Compassi-Severo 1, and Olympio L. Coutinho 1

¹Electronics Engineering Division, Electronic Warfare Laboratory (LAB-GE), Aeronautics Institute of Technology (ITA), São José dos Campos, Brazil

E-mail:, jose.melo.101783@ga.ita.br, {severolcs, olympio}@ita.br

Abstract

Modern space systems rely heavily on the Radio Frequency Direction Finder (RF DF) for various applications, where multichannel receivers are used to determine signal arrival angles. Accurate angle estimation requires precise front-end and signal processing. However, high-frequency electronics are susceptible to variations in electronic components due to manufacturing processes, temperature fluctuations, and voltage fluctuations, leading to errors. To mitigate these errors, amplitude and phase calibration of the multichannel front-end are crucial. This work presents and implements, using a Software Defined Radio (SDR), a simplified calibration technique for a dual-channel X-band RF front-end designed for space-based DF. The method involves applying a calibration signal to the front-end and measuring the amplitude and phase errors in the baseband signals using an SDR system. These measurements are used to create an error vector that is then applied in the software domain to compensate for system imbalances. Experimental validation was conducted within the 8.5 to 9.5 GHz X-band range, employing a modular dual-channel RF front-end connected to a dual-channel SDR, considering two scenarios of calibration in the software domain for the entire bandwidth.

Keywords: Direction Finder, Software Defined Radio, X-band Calibration, Space-Based Applications

1 Introduction

The capability of locating electromagnetic emitters and electronically target objects, enabled by *Direction Finders* (DF), is fundamental to the operation of numerous critical systems, from space and navigation technologies, rescue efforts, and beamforming antenna arrays applied in several applications [1, 2, 3, 4, 5, 6]. Knowing the position of an RF emitter can enhance system robustness, as demonstrated in [7], where direction-finding data improves the efficiency of maritime rescue operations. This is particularly valuable because environmental noise often obscures critical communication, and speakers may not share a common language.

The Angle of Arrival (AoA) estimation of electromagnetic waves or tracking beam direction changes in antenna arrays, can be achieved using various architectures. The simplest and most cost-effective approach employs a two-channel transceiver system, though accuracy generally improves with additional channels.

Beamforming and Direction Finding (DF) are typically pro-

cessed in the digital domain, as analog implementations require complex circuitry for phase shifting and triangulation. However, this digital approach demands precise compensation for front-end channel mismatches. Component variations introduce gain and phase errors between the antennas, which can degrade the accuracy of Direction of Arrival (DOA) estimation [8, 9].

Figure 1 presents the block diagram of the X-band DF system considered in this work. The architecture consists of a dual-channel X-band front-end and a two-channel software-defined radio (SDR). Each RF front-end channel is equipped with a Low-Noise Amplifier (LNA) and a mixer to translate the received signal from X-band to an intermediate frequency (IF). Following the front-end, the SDR further processes the signal. Inside the SDR, the received signals are amplified, down-converted from IF to quadrature baseband (BB) and converted from analog to digital. Thus, the I-Q digital data are delivered to a digital signal processor (DSP) and to the application serial bus [10].

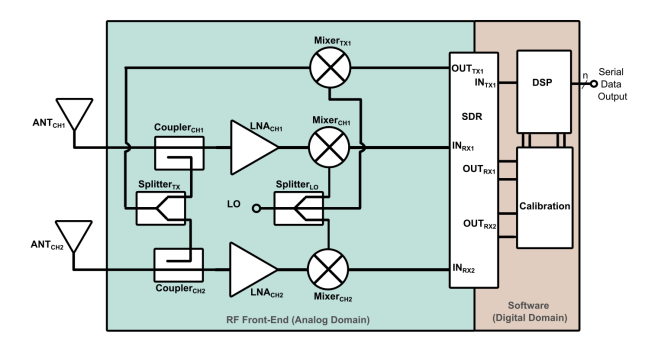


Figure 1: X-Band SDR-Based Direction Find Block Diagram.

To ensure system accuracy during operation, a real-time calibration system is integrated into the receiver. This is achieved by utilizing the SDR's transmitter and an up-converter mixer to generate a test signal. This test signal is then split and injected into the inputs of the receiver channels via two bidirectional couplers. This method allows coupling the calibration signal to the receiver inputs without degrading the receiver noise figure (NF) [11, 12]. The coupled reference signal enables the evaluation and subsequent compensation of gain and phase imbalances within the receiver chain, all performed in the digital/software domain.

Based on that, this paper analyses the capability of gain and phase calibration methods at the software domain for satellite receiver front-ends operating in the X-band. These analyses were performed through experiments with the RF front-end operating from 8.5 to 9.5 GHz using commercial monolithic microwave integrated circuits (MMICs) and a two-channel ADALM-PLUTO software-defined radio (SDR). The SDR data were processed using MATLAB and Python environments, and all measurements were made with standard microwave laboratory equipment.

This paper is organized as follows: Section II describes the theory of amplitude and phase calibration. Section III details the front-end design and SDR implementation. Section IV presents the experimental results, and Section V concludes this work.

2 Amplitude and Phase Calibration Analysis

To analyze the calibration process, the full diagram of Fig. 1 is redrawn as the simplified block diagram shown in Fig. 2 that represents the entire RF receiver path.

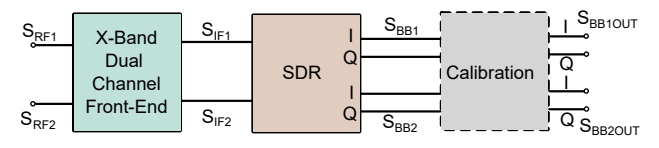


Figure 2: Simplified block diagram of the RF receiver

The dual-channel RF front-end receives the RF signals $S_{RF1/2}$ from the antennas and delivers the down-converted analog signals $S_{IF1/2}$ at an intermediate frequency (IF) to the software-defined radio (SDR). The SDR's quadrature receiver then processes these signals, down-converting them from IF

to baseband before they are sampled and converted to the digital domain.

The SDR's baseband output signals, $S_{BB1/2}$, are composed of In-phase $(I_{BB1/2})$ and Quadrature $(Q_{BB1/2})$ components and can be represented by their amplitude $(A_{BB1/2})$ and phase $(\phi_{BB1/2})$, as given by (1)

$$S_{BB1/2} = I_{BB1/2} + jQ_{BB1/2} = |A_{BB1/2}| \angle \phi_{BB1/2}$$
 (1)

The amplitude and phase of these signals can be obtained as follows:

$$|A_{BB1/2}| = \sqrt{I_{BB1/2}^2 + Q_{BB1/2}^2} \tag{2}$$

$$\phi_{BB1/2} = \arctan\left(\frac{Q_{BB1/2}}{I_{BB1/2}}\right) \tag{3}$$

Due to practical implementation imperfections such as differing path lengths and variations in active device gain, the baseband signals $(S_{BB1/2})$ will exhibit amplitude and phase imbalances. This mismatch occurs even when the same signal is applied to both RF inputs, necessitating a calibration system to compensate for the errors and be compatible with DF system use.

The calibration is performed by processing the received data in the baseband domain. Given a common RF input and local oscillator for both channels, the imbalances can be estimated. If Channel 1 is defined as the reference, the amplitude gain error is evaluated as the ratio of the signal amplitudes and the phase error is found from the phase difference between the channels, as expressed in (4) and (5).

$$\alpha_{BB12} = \frac{|A_{BB1}|}{|A_{BB2}|} \tag{4}$$

$$\Delta \phi_{BB12} = \phi_{BB1} - \phi_{BB2} \tag{5}$$

The calibration process utilizes the imbalance factors α_{BB12} and $\Delta\phi_{BB12}$ to correct the signals, with Channel 1 designated as the reference.

Two primary calibration methods were considered. The first approach corrects both the amplitude and phase of Channel 2 while applying a phase-only correction to Channel 1 to center the relative phase error. The second, simpler method applies the entire correction solely to Channel 2. Although the second method may require more signal samples to converge for large phase imbalances, it was adopted in this work due to its straightforward implementation. The resulting calibrated signals, S_{BB1}^* and S_{BB2}^* , are given by equations (6) and (7).

$$S_{BB1}^* = |A_{BB1}|e^{j(\phi_{BB1})} \tag{6}$$

$$S_{RB2}^* = \alpha_{BB12} |A_{BB2}| e^{j(\phi_{BB2} + \Delta\phi_{BB12})}$$
 (7)

A key challenge for the intended application is that the required 1 GHz of RF bandwidth in the X-band exceeds the instantaneous channel bandwidth of the SDR adopted in this work (up to 20 MHz). To address this, the wide spectrum is processed by splitting it into several narrower sub-bands. This

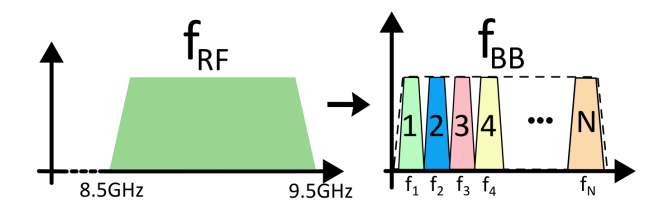


Figure 3: Frequency down-conversion process and the representation of the base-band signal in N narrow-band channels.

is achieved by systematically changing the center frequency of the SDR to select the desired frequency. In other words, the SDR cannot receive the entire signal bandwidth. Thus, the SDR will need to select the signal using individual channels according to its channel bandwidth limitation. It is depicted in Figure 2 when the RF bandwidth will be split into N time-multiplexed narrow-band channels. Consequently, gain and phase imbalance calibration must be performed independently for each sub-band. This is necessary because the frontend and SDR's characteristics are frequency-dependent and change with the center frequency of each segment.

During preliminary experimental testing, it was observed that the used SDR executes an internal re-initialization sequence each time its local oscillator frequency is changed. This sequence appears to alter the internal state of the device, causing previously acquired calibration data to become invalid. Crucially, returning to a previously calibrated frequency point does not restore the prior calibrated state. Consequently, a static or offline calibration approach is insufficient. The required solution is to implement a real-time calibration system that recalibrates the channels whenever the SDR's local oscillator frequency is adjusted.

3 X-Band Dual-Chanel RF Receiver System

The experimental results presented in this work were based on the circuit shown in Figure 1. The X-band RF dual channel front-end is composed of two MOD 415C-20 directional couplers ($Coupler_1$ and $Coupler_2$), two AFS4-08500960-18-10P-4 modular LNAs (LNA_1 and LNA_2), two PE8652 modular passive mixers ($Mixer_1$ and $Mixer_2$). The RF front-end is designed to operate in the X-band from 8.5 to 9.5 GHz. Biased with a +15 V power supply, it provides a nominal power gain of 24 dB and has a noise figure (NF) of 0.8 dB.

The SDR used in this work is an ADALM-PLUTO (Revision C), which is based on the Analog Devices AD9363 integrated transceiver. This single chip contains the complete dual-channel receiver path, and for this work, the device was specially configured to enable simultaneous operation of both receive channels. Figure 4 shows a simplified block diagram of front-end connected to the SDR. The receiver path includes the input preamplifiers ($LNA_{SDR1/2}$), down-conversion mixers with a variable local oscillator, tunable channel filters (up to 20 MHz bandwidth), and a 12-bit, 61.44 MS/s ($\frac{61.44}{2}$ MS/s for two channel operation) analog-to-digital converter (ADC). Digital data is delivered to the host computer via a USB 2.0

Table 1: Frequency of the local oscillator used to select the 200 MHz sub-bands.

LO Frequency (GHz)	RF bandwidth (GHz)		
8.1	8.5 - 8.7		
8.3	8.7 - 8.9		
8.5	8.9 - 9.1		
8.7	9.1 - 9.3		
8.9	9.3 - 9.5		

connection.

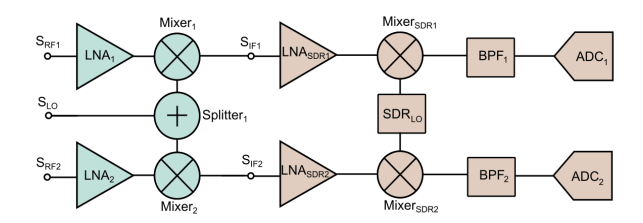


Figure 4: Schematic of the X-band front-end and simplified SDR block diagram used in this work.

For the TX calibration channel, we used the RF-80 C1 mixer $(Mixer_3)$ for up conversion and the PE2084 power splitter $(Splitter_1)$.

The usable bandwidth for each sub-band is determined by the system's intermediate frequency capabilities. The front-end mixer can produce an output signal up to 600 MHz, while the ADALM-PLUTO SDR's tunable range begins at 325 MHz. This establishes a usable IF bandwidth of 200 MHz for each segment, beginning at 400 MHz up to 600 MHz. To allow receiving the entire 8.5 GHz to 9.5 GHz the local oscillator (LO) signal (S_{LO}) is adjusted according to Table 1. to select the five distinct 200 MHz RF bands.

Additionally, the SDR is configured to a 10 MHz channel bandwidth. Thus, each of the five bands is further subdivided into 20 adjacent sub-bands. This results in a total of 100 channels of 10 MHz that can be considered in the 1 GHz bandwidth DF system.

4 Experimental Analysis

The experimental validation of the X-band DF system was conducted in our microwave laboratory using the equipment set shown in Fig. 5.

The setup uses one Agilent E8257D signal generator to provide the external local oscillator (S_{LO}) signal and an Agilent E3632A to supply DC bias to the front-end. The ADALM-PLUTO SDR, connected to a computer via USB 2.0, serves as the digital back-end.

For real-time calibration, the ADALM-PLUTO's TX output is split and routed back to both RX inputs to create a common reference signal. To independently verify performance, the output of the second receiver channel (RX2) is also split, sending the signal to the SDR and a Keysight N9042B signal

analyzer for monitoring.

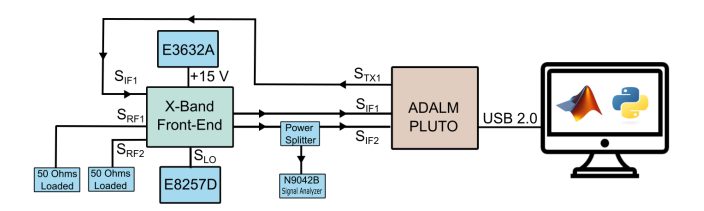


Figure 5: Equipment setup for the calibration measurements.

The data acquisition processed was performed with Python. Following data collection, the raw signals were exported to MATLAB for post-processing and analysis, where imbalance calculations and calibration corrections were performed. A photograph of the assembled laboratory setup is shown in Figure 6.

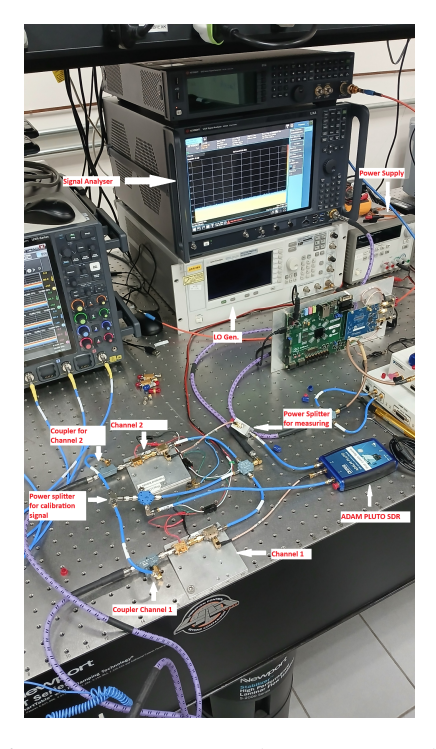


Figure 6: Equipment setup used in experimental results.

The measurement methodology involved first generating a set of calibration factors and then validating their effectiveness over the 8.5 GHz to 9.5 GHz RF band. Initially, a calibration signal (Signal 1) was swept across the band to create a correction matrix. Subsequently, the validity of this matrix was tested by applying the stored correction factors to two new, independent signals (Signal 2 and Signal 3) that were also swept across the same frequency range.

The results of this process are shown in Figure 7. The figure compares the initial uncalibrated response of Signal 1 against the ideally corrected case (where the calibration is applied to Signal 1 itself) and the corrected responses of the two validation signals.

As shown in a preliminary test, an initial attempt to use a static calibration matrix—generated from one signal sweep

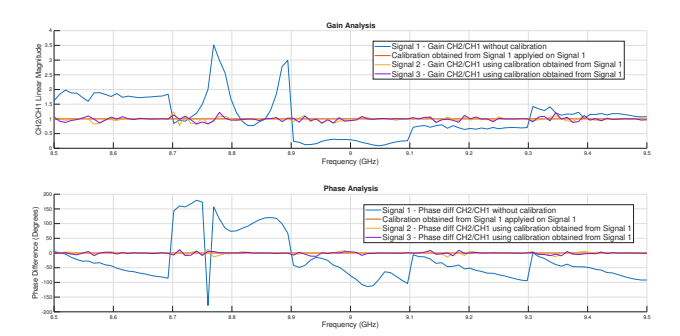


Figure 7: Gain and phase imbalance measurement for offline calibration.

and applied to others—proved ineffective as significant errors for direction finding remained.

It was first hypothesized that these errors were caused by transient effects in the system. To test this, a two-second delay was introduced before each measurement, but the errors persisted. Further analysis revealed the root cause to be an internal re-initialization sequence within the ADALM-PLUTO AD9363. This sequence is triggered by any change in the LO frequency or sample rate and appears to be non-deterministic; returning to a previous configuration does not guarantee a return to the same internal state, thus invalidating static calibration data.

To overcome this issue, a second methodology based on realtime, "in-place" calibration was adopted. This method consists of the following steps at a single, fixed frequency: 1) A signal is transmitted and its response is captured. 2) A calibration factor is calculated from this initial measurement. 3) The factor is immediately applied to a second and third measurement of the same continuous signal, each taken after a one-second delay, to evaluate the short-term stability and effectiveness of the correction. The results of this successful real-time methodology are presented in Figure 8.

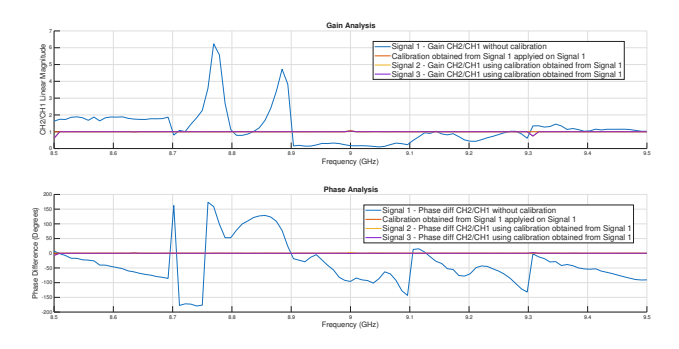


Figure 8: Gain and phase imbalance measurement for online calibration.

A comparison between Figure 7 (offline method) and Figure 8 (online method) highlights the significant difference in performance between the two approaches.

The statistical analysis shown in Tables 2, 3, 4, 5 comparing the Offline and Online calibration methods reveals a substantial difference in measurement consistency and repeatability, despite both systems successfully shifting the mean Amplitude Ratio and Phase Error close to their ideal target values (1.0 and 0.0°, respectively). For the Amplitude Ratio Error, the Online Calibration demonstrated far superior consistency, achieving a Standard Deviation (Std. Dev.) of only 0.003 on the same signal, compared to the 0.070 observed in the Offline method under new signal conditions. This stability advantage is even more pronounced in the Phase Error analysis, where the Online approach achieved a residual Std. Dev. as low as 0.06°, drastically outperforming the Offline method's residual Std. Dev. of approximately 4.0°. This data confirms that the enhanced synchronization and control provided by the Online architecture lead to significantly reduced residual error, establishing the Online Calibration as the superior method for maximizing precision and long-term measurement consistency.

Table 2: Statistical Analysis of the Amplitude Ratio Error for offline Calibration.

Measurement Step	Max	Min	Mean	Std. Dev.
Initial (Uncalib.)	3.518	0.085	1.099	0.700
Calibrated Data 2	1.238	0.774	0.989	0.067
Calibrated Data 3	1.223	0.826	0.991	0.070

Table 3: Statistical Analysis of the Phase Error (in Degrees) for offline Calibration.

Measurement Step	Max	Min	Mean	Std. Dev.
Initial (Uncalib.)	179.50	-178.97	-22.24	76.54
Calibrated Data 2	12.25	-13.99	-0.13	4.06
Calibrated Data 3	11.22	-11.26	-0.81	4.01

Table 4: Statistical Analysis of the Amplitude Ratio Error for online Calibration.

Measurement Step	Max	Min	Mean	Std. Dev.
Initial (Uncalib.)	6.238	0.096	1.248	1.046
2nd Reading	1.026	0.997	1.000	0.003
3rd Reading	1.092	0.614	0.994	0.046

Table 5: Statistical Analysis of the Phase Error (in Degrees) for online Calibration.

Measurement Step	Max	Min	Mean	Std. Dev.
Initial (Uncalib.)	173.59	-179.34	-36.15	74.32
2nd Reading	0.33	-0.32	0.00	0.06
3rd Reading	3.12	-7.47	0.01	0.83

5 Conclusion

This paper presented the development and validation of a calibration technique for a dual-channel X-band receiver intended for direction-finding applications. A key contribution of this work was the identification of a critical limitation in

conventional offline calibration approaches when using SDRs like the ADALM-PLUTO. This challenge is particularly significant because, unlike traditional narrowband direction finders that operate at a static frequency, our application requires finding the position of any signal source appearing within a wide 1 GHz bandwidth (8.5 to 9.5 GHz).

To overcome this challenge, a real-time, "in-place" calibration methodology was proposed and successfully implemented. This approach proved effective at correcting the significant gain and phase imbalances at discrete frequency points, validating its suitability for systems requiring frequency agility.

In future work, we intend to physically implement the hardware to fit within a 1U CubeSat standard and to add two corner antennas to evaluate DF performance in AoA estimation.

6 Acknowledgment

The authors would like to thank the FINEP and CNPq (grant 303609/2023-0) research agencies for the partial support of this work.

References

- [1] Luisa de la Fuente, Beatriz Aja, Enrique Villa, and Eduardo Artal. Calibration of a polarimetric microwave radiometer using a double directional coupler. *Remote Sensing*, 13(11):2109, may 2021. Online published: 28 May 2021.
- [2] Qi Wang, Yusong Liu, Yue Qin, Hao Guo, and Jun Tang. Microwave passive direction-finding method based on nv color center in diamond. *Micromachines*, 14(4):774, March 2023.
- [3] Mudassir Raza and Koji Tanaka. Demonstration of digital retrodirective method for solar power satellite. *Aerospace*, 10(4):498, February 2021.
- [4] Gustaw Mazurek and Rafał Rytel-Andrianik. Pilotbased calibration of dual-tuner SDR receivers. In 2020 28th European Signal Processing Conference (EU-SIPCO), pages 1971–1975, 2021.
- [5] Ibrahim Elshafiey, Abdel-Fattah Sheta, Mubashir Alam Nizam Uddin, Wazie M. Abdulkawi, and Waqar A. Malik. Adaptive energy concentration in hyperthermia treatment of cancer. In 2019 IEEE Asia-Pacific Conference on Applied Electromagnetics (APACE), pages 1–5, 2019.
- [6] Ümit Cezmi Yılmaz and Ümit Güler. On orbit demonstration of pointing accuracy of ground antennas by a flying GEO satellite. *Sakarya University Journal of Computer and Information Sciences*, 6(1):32–36, 2023.
- [7] Ole John and Maximilian Reimann. Increasing quality of maritime communication through intelligent speech recognition and radio direction finding. In 2020

- European Navigation Conference (ENC), pages 1-7, 2020.
- [8] Aifei Liu, Guisheng Liao, Cao Zeng, Zhiwei Yang, and Qing Xu. An eigenstructure method for estimating DOA and sensor gain-phase errors. *IEEE Transactions on Signal Processing*, 59(12):5944–5956, 2011.
- [9] Wei Xie, Changsheng Wang, Fei Wen, Jiangbo Liu, and Qun Wan. DOA and gain-phase errors estimation for noncircular sources with central symmetric array. *IEEE Sensors Journal*, 17(10):3068, 2017.
- [10] Daniel Gaydos, Payam Nayeri, and Randy Haupt. Calibration and synchronization of software-defined-radio arrays. In 2020 IEEE International Symposium on Antennas and Propagation and North American Radio Science Meeting, pages 2075–2076, 07 2020.
- [11] Björn Debaillie, Peter Van Wesemael, and Jan Craninckx. Calibration method enabling low-cost SDR. In *Proceedings of IEEE International Conference on Communications, ICC 2008, Beijing, China, 19-23 May 2008*, pages 4899–4903. IEEE, 2008.
- [12] Björn Debaillie, Peter Wesemael, and Jan Craninckx. Calibration of SDR circuit imperfections. In 2008 IEEE Global Telecommunications Conference (GLOBECOM), pages 4700–4704, 01 2008.